AGU PUBLICATIONS

Geophysical Research Letters

RESEARCH LETTER

10.1002/2014GL062888

Key Points:
- Iron-bearing bridgmanite
- Elasticity
- Pressure-induced iron state change

Supporting Information:
- Text S1
- Figure S1
- Figure S2
- Figure S3
- Figure S4

Correspondence to:
G. Shukla and R. M. Wentzcovitch,
shukla@physics.umn.edu;
wentz002@umn.edu

Citation:
Shukla, G., Z. Wu, H. Hsu, A. Floris, M. Cococcioni, and R. M. Wentzcovitch (2015), Thermoelasticity of Fe^{2+}-bearing bridgmanite, *Geophys. Res. Lett.*, *42*, 1741–1749, doi:10.1002/2014GL062888.

Received 20 DEC 2014
Accepted 23 FEB 2015
Accepted article online 25 FEB 2015
Published online 24 MAR 2015

Thermoelasticity of Fe^{2+}-bearing bridgmanite

Gaurav Shukla[1], Zhongqing Wu[2], Han Hsu[3], Andrea Floris[4], Matteo Cococcioni[5], and Renata M. Wentzcovitch[1,6]

[1]School of Physics and Astronomy, University of Minnesota, Twin Cities, Minneapolis, Minnesota, USA, [2]School of Earth and Space Sciences, University of Science and Technology of China, Hefei, China, [3]Department of Physics, National Central University, Taoyuan, Taiwan, [4]Department of Physics, King's College London, London, UK, [5]Theory and Simulation of Materials (THEOS), École Polytechnique Fédérale de Lausanne, Lausanne, Switzerland, [6]Department of Chemical Engineering and Materials Science, University of Minnesota, Twin Citites, Minneapolis, Minnesota, USA

Abstract We present local density approximation augmented by the Hubbard-type correction calculations of high-temperature elastic properties of bridgmanite with composition $(Mg_{(1-x)}Fe^{2+}_x)SiO_3$ for $0 \leq \times \leq 0.125$. Results of elastic moduli and acoustic velocities for the Mg end-member ($x = 0$) agree very well with the latest high-pressure and high-temperature experimental measurements. In the iron-bearing system, we focus particularly on the change in thermoelastic parameters across the state change that occurs in ferrous iron above ~30 GPa, often attributed to a high-spin (HS) to intermediate-spin (IS) crossover but explained by first-principles calculations as a lateral displacement of substitutional iron in the perovskite cage. We show that the measured effect of this change on the equation of state of this system can be explained by the lateral displacement of substitutional iron and not by the HS to IS crossover. The calculated elastic properties of $(Mg_{0.875}Fe^{2+}_{0.125})SiO_3$ along an adiabatic mantle geotherm somewhat overestimate longitudinal velocities but produce densities and shear velocities quite consistent with the Preliminary Reference Earth Model data throughout most of the lower mantle.

1. Introduction

Thermoelastic properties of lower mantle minerals provide a direct link to seismological observations. In order to constrain the composition and thermal structure of the Earth's lower mantle, a detailed investigation of elastic properties of the constituent minerals is needed. Bridgmanite, $(Mg,Fe,Al)(Si,Fe,Al)O_3$ perovskite (Pv), is the main constituent of the lower mantle along with (Mg,Fe)O ferropericlase, $CaSiO_3$ perovskite, and $(Mg,Fe,Al)(Si,Fe,Al)O_3$ postperovskite (PPv). Although there has been considerable progress in measurements of elastic properties of these minerals at high pressures and temperatures [*Yeganeh-Haeri*, 1994; *Sinnelnikov et al.*, 1998; *Fiquet et al.*, 2000; *Andrault et al.*, 2001; *Aizawa et al.*, 2004; *Jackson et al.*, 2004, 2005b; *Sinogeikin et al.*, 2004; *Li and Zhang*, 2005; *Murakami et al.*, 2007; *Lundin et al.*, 2008; *Boffa Ballaran et al.*, 2012; *Chantel et al.*, 2012; *Murakami et al.*, 2012; *Dorfman et al.*, 2013], owing to extreme pressure and temperature conditions in the lower mantle, the availability of data on Fe-bearing bridgmanite is quite limited to well-constrained lower mantle composition and temperature. Several experiments and first-principles calculations have shown that pressure-induced iron spin crossover [*Badro et al.*, 2003, 2004; *Tsuchiya et al.*, 2006; *Lin et al.*, 2012] affects elastic properties of (MgFe)O ferropericlase (fp) [*Goncharov et al.*, 2006; *Crowhurst et al.*, 2008; *Marquardt et al.*, 2009; *Wentzcovitch et al.*, 2009; *Wu et al.*, 2009; *Antonangeli et al.*, 2011; *Wu et al.*, 2013; *Wu and Wentzcovitch*, 2014]. In the case of iron-bearing bridgmanite, effects of spin crossover on elastic properties have been quite uncertain due to possible coexistence of ferrous (Fe^{2+}) and ferric (Fe^{3+}) iron along with the more complex perovskite crystal structure. Experimentally, it has been difficult to isolate the effects of ferrous and ferric iron unambiguously.

Acoustic velocity measurements using an ultrasonic technique [*Chantel et al.*, 2012] and compression curve measurements [*Boffa Ballaran et al.*, 2012] in iron-bearing bridgmanite demonstrated a significant change in bulk modulus across the state change in iron. By fitting experimental data with third-order Birch-Murnaghan equation of state to small (0–40 GPa) and large (0–75 GPa) pressure ranges, *Boffa Ballaran et al.* [2012] found ambient condition bulk modulus smaller (245 GPa) and larger (253 GPa), respectively. Since these fitting pressure ranges had no effect on the iron-free phase, *Boffa Ballaran et al.* [2012] attributed this behavior to change in compression mechanism caused by the high-spin (HS) to intermediate-spin (IS) crossover [*McCammon et al.*, 2008]. However, the HS to IS crossover has not been found in first-principle

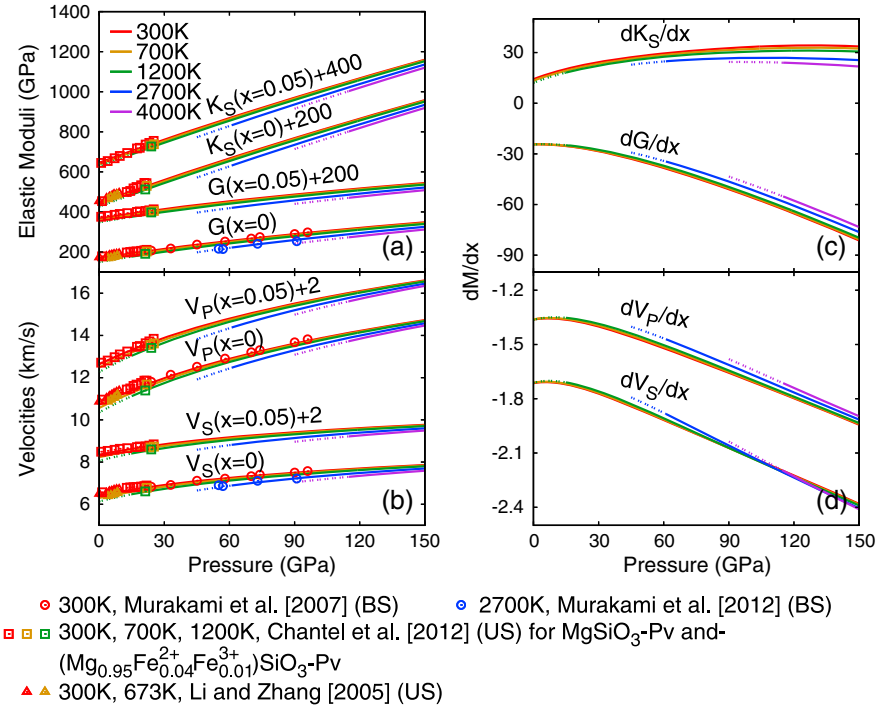

Figure 1. Pressure and temperature dependence of (a) elastic moduli and (b) sound velocities for $(Mg_{1-x}Fe_x^{2+})\,SiO_3$ with $x = 0$ and 0.05 and of (c, d) dM/dx ($M = K_S, G, V_P, V_S$). Solid (dashed) lines represent first-principles results within (outside) the validity of quasi-harmonic approximation. BS: Brillouin scattering, US: ultrasonic technique.

studies [*Bengtson et al.*, 2009; *Hsu et al.*, 2010, 2011; *Hsu and Wentzcovitch*, 2014]. Using the local density approximation augmented by the Hubbard-type correction (LDA + U) method, *Hsu et al.* [2010] showed that iron in Fe^{2+}-bearing bridgmanite should remain in the HS state throughout the lower mantle and should, instead, undergo a pressure-induced displacement producing a state with increased iron Mössbauer quadrupole splitting (QS). The calculated low (1.9–2.4 mm/s) and high (3.3–3.9 mm/s) QS states were consistent with experimental measurements [*Lin et al.*, 2012; *McCammon et al.*, 2008, 2013; *Potapkin et al.*, 2013; *Kupenko et al.*, 2014]. Owing to lack of sufficient experimental measurements on elasticity of iron-bearing bridgmanite, effects of the proposed HS to IS crossover [*McCammon et al.*, 2008], or iron displacement [*Bengtson et al.*, 2009; *Hsu et al.*, 2010, 2011; *Hsu and Wentzcovitch*, 2014], have not been properly understood. To clarify this issue, we have calculated the high-temperature and high-pressure elastic moduli and acoustic velocities of $(Mg_{1-x}Fe_x)SiO_3$ for $x = 0$ and $x = 0.125$, with iron in low- and high-QS states. We also compare the effects of the HS to IS transition [*Hsu and Wentzcovitch*, 2014] in the static equation of state of Fe^{2+}-bearing bridgmanite.

Unlike in $(MgFe^{3+})(SiFe^{3+})O_3$ [*Hsu et al.*, 2011], the high-spin (HS) to low-spin (LS) transition in $(MgFe^{2+})SiO_3$ has not been found in the lower mantle pressure range using the LDA + U method [*Hsu et al.*, 2010; *Hsu and Wentzcovitch*, 2014]. However, there have been several studies suggesting that HS to LS transition might occur at around ~90 GPa [*Badro et al.*, 2004; *Li et al.*, 2004, 2006; *Jackson et al.*, 2005a; *McCammon et al.*, 2008; *Umemoto et al.*, 2008; *Lin et al.*, 2012] and might have consequences for the vibrational spectrum [*Caracas et al.*, 2014]. Recently, *Zhang et al.* [2014] found that iron-bearing bridgmanite dissociates into nearly iron-free phase and into an iron-rich hexagonal silicate phase in the deep lower mantle. As the dissociation phase boundary is still not well known, we present results for elasticity of Fe^{2+}-bearing bridgmanite with constant iron concentration in the entire pressure range of the lower mantle.

2. Method and Calculation Details

We have used density functional theory (DFT) [*Hohenberg and Kohn*, 1964; *Kohn and Sham*, 1964] within the local density approximation (LDA) [*Ceperley and Alder*, 1980] augmented by the Hubbard U (LDA + U) calculated self-consistently [*Cococcioni and de Gironcoli*, 2005; *Kulik et al.*, 2006; *Hsu et al.*, 2009; *Leiria Campo*

Table 1. Volume, Sound Velocities, Elastic Moduli, and Their Pressure Derivatives at Ambient Pressure and Temperature Conditions[a]

V (Å^3)	x	V_P (km/s)	V_S (km/s)	K_S (GPa)	G (GPa)	K'	G'	References
163.2	0	10.72	6.42	245.5	168.2	3.96	1.79	This study, single crystal/LDA
163.3	0.05	10.63	6.34	245.8	167.02	4.03	1.79	This study, single crystal/LDA+U (low QS)
162.3(0.6)	0	11.04	6.57	264(5)	177(4)	-	-	*Yeganeh-Haeri* [1994], single crystal/BS
162.3	0	-	6.51	-	176(5)	-	1.8(0.4)	*Sinnelnikov et al.* [1998], polycrystal/US
162.4(0.5)	0	10.84(0.1)	6.47(0.06)	253(5)	173(3)	-	-	*Sinogeikin et al.* [2004], polycrystal/BS
162.4(0.5)	0	10.88(0.06)	6.54(0.03)	253(3)	175(2)	-	-	*Sinogeikin et al.* [2004], single crystal/BS
162.3	0	10.86(0.05)	6.49(0.04)	253(2)	173(1)	4.4(0.1)	2.0(0.1)	*Li and Zhang* [2005], polycrystal/US
-	0	10.85(0.03)	6.49(0.03)	-	172.9(1.5)	-	1.56(0.04)	*Murakami et al.* [2007], polycrystal/BS
162.2(0.2)	0	10.82(0.06)	6.54(0.04)	247(4)	176(2)	4.5(0.2)	1.6(0.1)	*Chantel et al.* [2012], polycrystal/US
166.5(0.2)	0.05	10.60(0.06)	6.46(0.04)	236(2)	174(1)	4.7(0.1)	1.56(0.5)	*Chantel et al.* [2012], polycrystal/US
162.4	0	-	-	267	180	4.10	-	*Oganov et al.* [2001], simulations
162.49	0	-	-	269(2)	159(2)	-	-	*Marton and Cohen* [2002], simulations
162.4	0	-	-	250.5	172.9	4.01	1.74	*Zhang et al.* [2013], simulations
				Compression Studies				
V (Å^3)				K_T		K'		
162.3	0			259.5		3.69		*Fiquet et al.* [2000]
162.4	0			248.8		4		*Andrault et al.* [2001]
162.7	0.05			255.4		4		*Andrault et al.* [2001]
164.1	0			247		3.97		*Karki et al.* [2001], simulations
162.30	0			255–261		4		*Lundin et al.* [2008]
162.18	0.09			257–259		4		*Lundin et al.* [2008]
163.30	0.15			257–259		4		*Lundin et al.* [2008]
163.09(0.06)	0.04			253(2)		3.99(0.07)		*Boffa Ballaran et al.* [2012], (0–75 GPa)
163.16(0.06)	0.04			245(4)		4.4(0.03)		*Boffa Ballaran et al.* [2012], (0–40 GPa)
166.5(0.2)	0.05			246(2)		4		*Chantel et al.* [2012],
163.0	0.09			251(13)		4		*Dorfman et al.* [2013]

[a]BS: Brillouin scattering; US: ultrasonic; XRD: X-ray diffraction.

and Cococcioni, 2010; *Himmetoglu et al.*, 2014]. Ultrasoft pseudopotentials [*Vanderbilt*, 1990] have been used for Fe, Si, and O. For Mg, a norm-conserving pseudopotential generated by von Barth-Car's method has been used. A detailed description about pseudopotentials is available in *Umemoto et al.* [2008]. The plane wave kinetic energy and charge density cutoff are 40 Ry and 160 Ry, respectively. Structural optimization at arbitrary volumes has been performed using variable cell-shape damped molecular dynamics [*Wentzcovitch*, 1991; *Wentzcovitch et al.*, 1993]. Self-consistent and structurally consistent $U_{sc} = 3.1$ eV, reported by *Hsu et al.* [2010] using the linear response approach [*Cococcioni and de Gironcoli*, 2005; *Kulik et al.*, 2006], has been used for high-spin low-QS and high-QS iron. Vibrational density of states (VDoS), needed to calculate free energy within quasi-harmonic approximation [*Carrier et al.*, 2007], have been calculated using density functional perturbation theory [*Baroni et al.*, 2001] using the LDA + U functional [*Floris et al.*, 2011]. $(Mg_{1-x}Fe_x)SiO_3$ for $x = 0$ and 0.125 have been investigated in a 40-atom supercell. Elastic properties for $0 < \times < 0.125$ are linearly interpolated using $x = 0$ and $x = 0.125$ results. Electronic states have been sampled on $2 \times 2 \times 2$ Monkhorst-Pack k-point grid shifted by $(1/2, 1/2, 1/2)$ from the Brillouin zone origin. VDoS have been obtained by calculating dynamical matrices on a $2 \times 2 \times 2$ q-point grid and interpolating the obtained force constants on an $8 \times 8 \times 8$ q-point grid. The structure for $x = 0$ and $x = 0.125$ with high-QS state have been optimized at 12 pressures between −10 and 150 GPa. The low-QS structure has been optimized up to 60 GPa only. Beyond this pressure unstable phonons appear. To obtain static elastic coefficients (zero temperature), C_{ij}, at each pressure, positive and negative strains of 1% magnitude have been applied, and after relaxing the internal degrees of freedom, associated stresses have been calculated. Thermoelastic moduli have been calculated using a semianalytical approach [*Wu and Wentzcovitch*, 2011]. This method uses an analytical expression for strain Grüneisen parameters to calculate the thermal contribution to

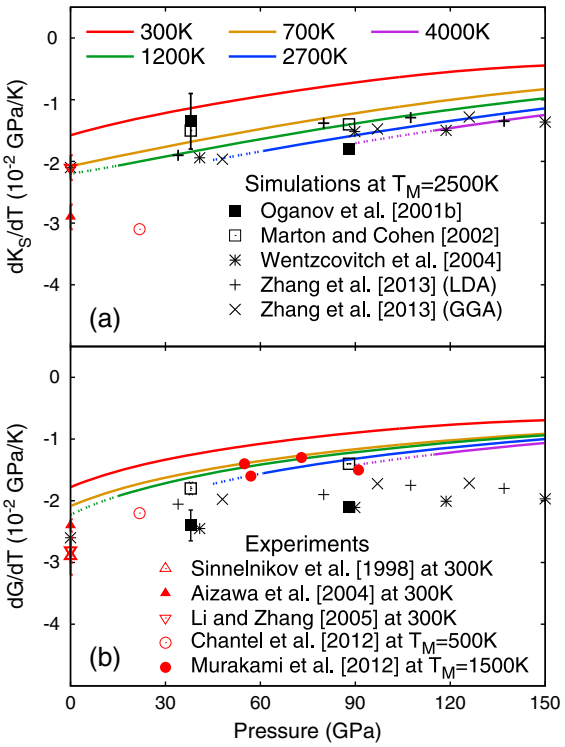

Figure 2. Pressure and temperature dependence of (a) $\frac{dK_S}{dT}$ and (b) $\frac{dG}{dT}$ for iron-free bridgmanite. Results from this study (lines) are compared with previous simulations (black symbols) and experimental data (red symbols). The values of $\frac{dK_S}{dT}$ and $\frac{dG}{dT}$ obtained from previous simulations [*Oganov et al.*, 2001; *Marton and Cohen*, 2002; *Wentzcovitch et al.*, 2004; *Zhang et al.*, 2013] and experimental measurements [*Chantel et al.*, 2012; *Murakami et al.*, 2012] shown here are calculated at the midpoint between extreme temperatures (i.e., $\frac{dM(P,T_M)}{dT} = \frac{M(P,T_2)-M(P,T_1)}{T_2-T_1}$, where $T_M = \frac{T_1+T_2}{2}$ and $M = (K_S, G)$). Error bars on *Oganov et al.* [2001] and *Marton and Cohen* [2002] results are reproduced from *Zhang et al.* [2013], while on *Wentzcovitch et al.* [2004] and *Zhang et al.* [2013] they are smaller than the size of the symbols.

elastic coefficients using the quasi-harmonic approximation. This method allows calculations of thermal elastic coefficients using static values and vibrational density of states for unstrained configurations only. It is almost 2 orders of magnitude more efficient than the fully numerical method [*Karki et al.*, 1999; *Wentzcovitch et al.*, 2004], which required vibrational density of states also for strained configurations. It also appears to be more accurate since it avoids numerical differentiation on a reduced number of grid points as well as calculations of VDoS and free energies for strained configurations. The method has been applied successfully to several minerals already [*Wu and Wentzcovitch*, 2011; *Nunez–Valdez et al.*, 2012a, 2012b, 2013; *Yang and Wu*, 2014]. Calculations have been performed using VLab cyberinfrastructure at the Minnesota Supercomputing Institute [*da Silva et al.*, 2008].

3. Results and Discussion

3.1. Elasticity of Iron-Free and Fe^{2+}-Bearing Bridgmanite

The calculated aggregate elastic moduli, K and G, and acoustic velocities, V_P and V_S, of iron-free bridgmanite compare well with Brillouin scattering measurements of *Murakami et al.* [2007, 2012] as shown in Figures 1a and 1b. Within experimental uncertainties, ultrasonic measurements of *Li and Zhang* [2005] and *Chantel et al.* [2012] also compare well with our results. Table 1 compares calculated elastic properties at zero pressure and 300 K with measurements and simulations at ambient conditions. As compared to experimental measurements, our calculated volume is overestimated by ~0.5%, while elastic moduli and acoustic velocities are underestimated by ~1–3% , which is typical for LDA calculations after including zero-point energy [*Karki et al.*, 1999, 2001; *Wentzcovitch et al.*, 2004, 2010a, 2001b]. Calculated pressure derivatives of elastic moduli, K' and G', are 3.96 and 1.79, respectively. Our K' agrees reasonably well with previous studies, while G' compares well with those reported by *Sinnelnikov et al.* [1998] and *Zhang et al.* [2013]. Comparing acoustic velocities and elastic moduli at higher temperatures, especially shear velocities and shear moduli at 2700 K by *Murakami et al.* [2012], we find that the temperature dependence of elastic properties has been captured well. As shown in Figure 2, our calculated $\frac{dK_S}{dT}$ and $\frac{dG}{dT}$ are smaller in magnitude compared to values obtained by ultrasonic [*Sinnelnikov et al.*, 1998; *Aizawa et al.*, 2004; *Li and Zhang*, 2005] at 0 GPa and Brillouin scattering measurements [*Chantel et al.*, 2012] at 22 GPa. Calculated values of $\frac{dK_S}{dT}$ compare well with those of previous calculations [*Oganov et al.*, 2001; *Marton and Cohen*, 2002; *Wentzcovitch et al.*, 2004; *Zhang et al.*, 2013]. Calculated $\frac{dG}{dT}$ agree well with Brillouin scattering measurements by *Murakami et al.* [2012] and nonself-consistent calculation by *Marton and Cohen* [2002] but differ substantially from that of *Oganov et al.* [2001], *Wentzcovitch et al.* [2004], and *Zhang et al.* [2013].

The semianalytical method used here had produced well the temperature dependence of elasticity for all applied materials [*Wu and Wentzcovitch*, 2011; *Nunez-Valdez et al.*, 2012a, 2012b, 2013; *Yang and Wu*, 2014].

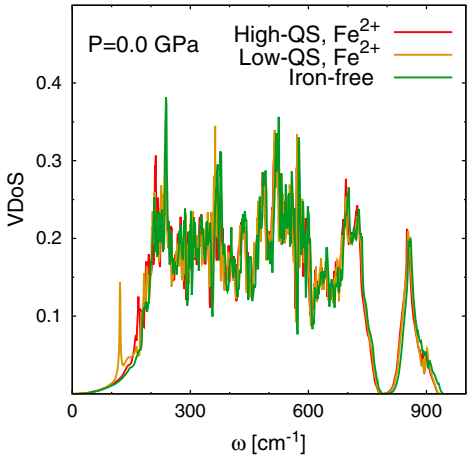

Figure 3. Vibrational density of states (VDoS) at $P = 0$ for iron-free bridgmanite using LDA and for low- and high-QS states of $(Mg_{0.875}Fe^{2+}_{0.125})\,SiO_3$ using LDA+U.

This method has also produced slightly better results for MgO [*Wu and Wentzcovitch*, 2011] than the fully numerical method [*Karki et al.*, 1999; *Wentzcovitch et al.*, 2004]. This is because this method avoids calculations of vibrational frequencies in strained configurations and numerical errors associated with finite difference calculations of elastic coefficients.

The elastic moduli and acoustic velocities of iron-bearing bridgmanite at lower mantle pressures are also shown in Figure 1. To compare with measurements of *Boffa Ballaran et al.* [2012] and *Chantel et al.* [2012] in the iron-bearing phase, we estimated elastic properties for $0 < x < 0.125$ by linearly interpolating our calculated results for $x = 0$ and $x = 0.125$. The calculated volume at ambient conditions is in agreement with measurements by *Boffa Ballaran et al.* [2012] for $x = 0.04$ and is smaller by ~2% when compared with measurements by *Chantel et al.* [2012] for $x = 0.05$ (Table 1). As shown in Figure 1b, comparison of calculated acoustic velocities, V_P and V_S, for $x = 0.05$ with the only available experimental measurements for $(Mg_{0.95}Fe^{2+}_{0.04}Fe^{3+}_{0.01})SiO_3$ [*Chantel et al.*, 2012] is also good except for the shear velocity data in the lower pressure range. As seen in Figures 1c and 1d and in Table 1, the presence of iron has very little to no effect on bulk modulus, K_S, but shear modulus G softens by ~2 to 6%, consistent with previous static first-principles studies [*Kiefer et al.*, 2002; *Lundin et al.*, 2008]. The effect of iron on the temperature dependence of acoustic velocities and elastic moduli is not very significant (see Figure 1).

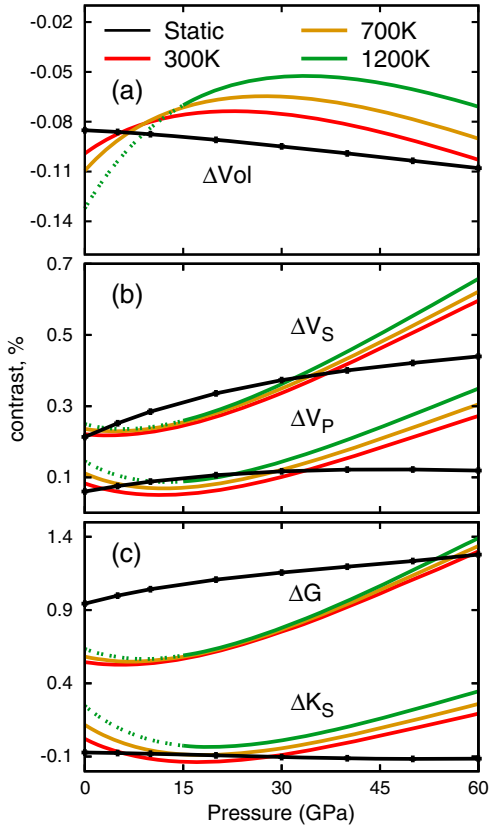

Figure 4. Contrast (ΔM) in (a) unit-cell volume, (b) compressional and shear velocity (V_P, V_S), and (c) bulk and shear modulus (K_S, G) between low-QS and high-QS states in $(Mg_{0.875}Fe^{2+}_{0.125})\,SiO_3$.

3.2. Effect of Pressure-Induced Iron Displacement on Elasticity

We have investigated the elastic consequences of the pressure-induced iron displacement [*Hsu et al.*, 2010; *Hsu and Wentzcovitch*, 2014] by calculating thermal elastic moduli and acoustic velocities for $x = 0.125$ with iron in low-QS and high-QS sites. The low-QS structure is stable up to 60 GPa in LDA+U calculations. Above this pressure unstable phonon modes start appearing. As shown in Figure 3, vibrational density of states (VDoS) for $x = 0$ and for $x = 0.125$ with iron in the high-QS and low-QS sites are not very different except for a small shift toward lower frequencies owing to the presence of iron. However, there is an extra peak at ~150 cm^{-1} in the VDoS if iron is in the low-QS site. It is worth noting that the vibrational mode associated with this extra peak in the low-QS structure is infrared active, while the same mode is infrared inactive in the high-QS structure. This information may provide a crucial test to investigate the states of ferrous iron in bridgmanite.

The effect of iron displacement (low-QS to high-QS transition) on unit-cell volume, acoustic velocities, and elastic moduli of iron-bearing bridgmanite with $x = 0.125$ is shown in Figure 4. To quantify the magnitude of the property change, we define the contrast Δ in a particular property M as

Table 2. Calculated Equation of State Parameters for Low QS, High QS, and Combined Results at 30 GPa for Low QS and High QS Fitted With Different Pressure Range

	300 K			700 K		
	V (Å^3)	K_T	K'	V (Å^3)	K_T	K'
Low QS	163.81	247.16	4.05	165.62	234.05	4.12
High QS	163.64	248.90	3.97	165.44	236.44	4.03
Combined data (0–150 GPa)	163.81	245.59	4.02	165.62	233.93	4.06
Combined data (0–90 GPa)	163.87	243.41	4.09	165.67	232.32	4.11
Combined data (0–75 GPa)	163.93	241.25	4.15	165.68	232.29	4.12

$\Delta M = \frac{M_{\text{high-QS}} - M_{\text{low-QS}}}{M_{\text{low-QS}}} \times 100$. As shown in Figure 4, the volume contrast is very small (~0.1%), consistent with *Lundin et al.* [2008] and *Boffa Ballaran et al.* [2012], and is unlikely to be detected in experiments. The contrast in bulk modulus, K_S, and acoustic velocities, V_P and V_S, are also small. However, the shear modulus contrast is about ~0.5–1.5%. This change in G was also suggested by *Boffa Ballaran et al.* [2012] using spontaneous strain analysis. To investigate the fitting pressure-range behavior observed by *Boffa Ballaran et al.* [2012] and *Chantel et al.* [2012], the calculated results for low QS and high QS have been combined at 30 GPa, the pressure above which the HS to IS crossover was proposed by *McCammon et al.* [2008] and *Potapkin et al.* [2013]. The third-order Birch-Murnaghan equation of state was used to fit these combined results. As shown in Table 2, depending on the pressure range of the combined results, an isothermal bulk modulus softening of ~3 to 7 GPa has been found. This softening, however, reduces with increasing temperature.

Intermediate-spin (IS) states of the iron in Fe^{2+}-bearing bridgmanite are energetically unfavored in the lower mantle pressure range [*Hsu et al.*, 2010; *Hsu and Wentzcovitch*, 2014], and phonon calculations have been extremely difficult for these states. To understand the overall trend of fitting parameters of combined low-QS and IS data, we have used static data for low-QS state and IS state with QS value 0.9–1.6 mm/s [*Hsu and Wentzcovitch*, 2014]. The static bulk modulus at zero pressure for low-QS and IS states are 263.2 GPa and 254.1 GPa, respectively (Figure S3 in the supporting information). When static low-QS and IS results have been combined at 30 GPa and fitted within different pressure ranges of 0–150 GPa and 0–120 GPa, static bulk modulus of the combined fit are 305 GPa and 348.7 GPa, respectively (Figure S4). The fitting pressure-range trend of combined low QS and high QS is the same as that observed by *Boffa Ballaran et al.* [2012] and *Chantel et al.* [2012], while of combined low-QS and IS states the fitting trend is opposite. These findings substantiate our understanding that ferrous iron in perovskite remains in the HS state in the lower mantle pressure range and instead undergoes a horizontal displacement in the perovskite cage which results in an increase in Mössbauer quadrupole splitting.

4. Geophysical Significance

As shown in Figure 5, elastic moduli (K_S, G), acoustic velocities (V_P, V_S), and densities (ρ) are calculated along the Boehler's geotherm [*Boehler*, 2000] using new [*Wu and Wentzcovitch*, 2011] and previous [*Karki et al.*, 1999; *Wentzcovitch et al.*, 2004] methods, and the results are compared with seismic values from the Preliminary Reference Earth Model (PREM) [*Dziewonski and Anderson*, 1981]. Owing to the smaller magnitude of $\frac{dG}{dT}$ obtained here, present results for G and V_s differ more from previous results by *Wentzcovitch et al.* [2004] in the deep lower mantle region, where temperatures are higher. This difference is sufficient to alter conclusions regarding mantle composition. Inclusion of 12.5% Fe^{2+} in $MgSiO_3$ perovskite produces good agreement of ρ, V_S, and G with PREM values (Figures 5c and 5d). Therefore, comparison of calculated V_S with PREM's V_S may indeed suggest a more perovskitic lower mantle [*Murakami et al.*, 2012]. However, relatively large values of K_S and V_P are found, suggesting that the lower mantle may accommodate a reasonable amount of ferropericlase, (MgFe)O, and $CaSiO_3$ perovskite as previously indicated [*Wentzcovitch et al.*, 2004]. Resolving whether the lower mantle composition is pyrolytic or perovskitic still needs more detailed investigations of the effect of Al_2O_3 and Fe_2O_3 on the elasticity of bridgmanite along with the elasticity of $CaSiO_3$ perovskite. Ultimately, the analysis of one-dimensional velocity profiles might be too limited to address this question more conclusively. Analysis of lateral heterogeneities, including effects of

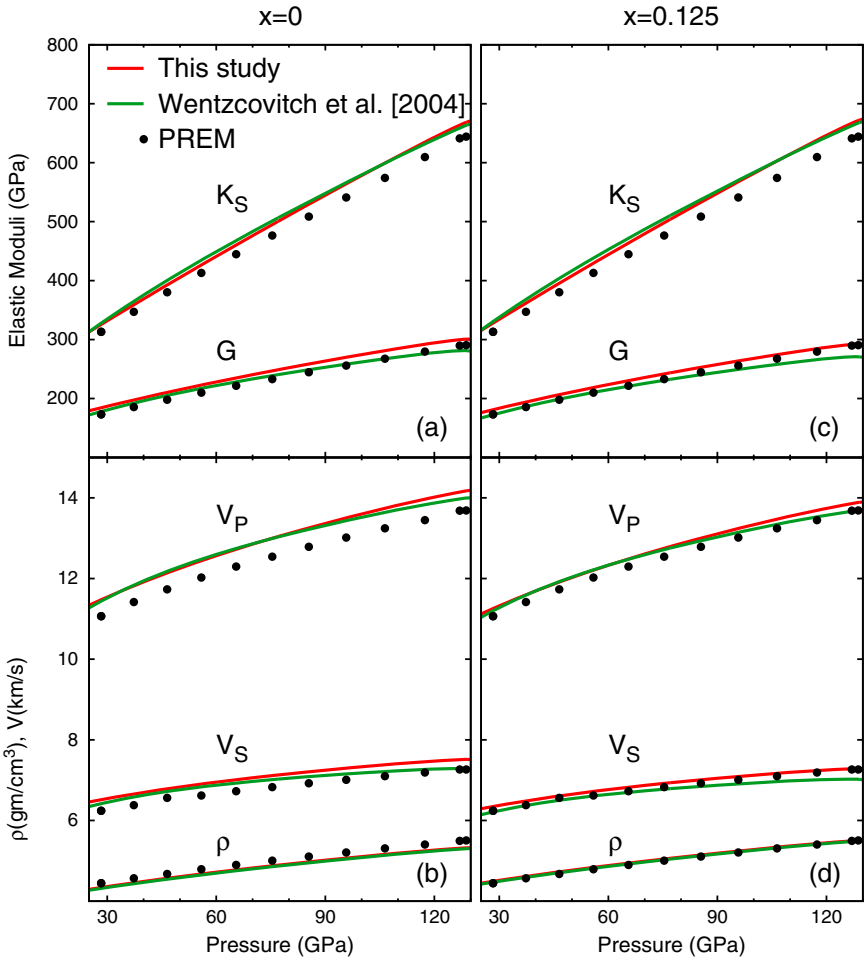

Figure 5. Elastic moduli (K_S, G), sound velocities (V_P, V_S), and density (ρ) for $\left(Mg_{1-x}Fe_x^{2+}\right)SiO_3$ with (a, b) $x=0$ and (c, d) $x=0.125$ calculated along the Boehler's geotherm [*Boehler*, 2000] using present [*Wu and Wentzcovitch*, 2011] and previous [*Wentzcovitch et al.*, 2004] methods.

spin crossovers in (MgFe)O [*Wu and Wentzcovitch*, 2014] and in bridgmanite, might prove more useful to address this question.

5. Conclusions

We have presented first-principles LDA + U calculations of aggregate elastic moduli and acoustic velocities for Fe^{2+}-bearing bridgmanite at lower mantle conditions. Using the new semianalytical approach for high-temperature elasticity [*Wu and Wentzcovitch*, 2011], we find an unexpected difference of temperature gradients with respect to previous fully numerical calculations [*Wentzcovitch et al.*, 2004] also based on the quasi-harmonic approximation. New results for $\frac{dG}{dT}$ and $\frac{dV_S}{dT}$ for iron-free bridgmanite are in good agreement with the latest high-temperature high-pressure measurements of these quantities by *Murakami et al.* [2012], which also differ from previous calculations and previous experiments. Overall, it appears that pressure and temperature gradients of bulk and shear moduli are better estimated now. Calculated acoustic velocities for iron-bearing bridgmanite also agree well with ultrasonic measurements of *Chantel et al.* [2012]. We do not find any significant effect of iron-site change (low QS to high QS) on sound velocities and elastic moduli, except for ~1% increase in shear modulus, consistent with findings by *Boffa Ballaran et al.* [2012]. Effects of fitting combined data for low-QS and high-QS states on elastic properties are consistent with fitting pressure-range behavior previously observed by *Boffa Ballaran et al.* [2012] and *Chantel et al.* [2012]. Calculated shear modulus and shear velocities of bridgmanite along a typical mantle geotherm are qualitatively more consistent with PREM values now compared with previous first-principles results [*Wentzcovitch et al.*, 2004]. Differences in bulk modulus and longitudinal velocities remain noticeable.

Acknowledgments
This work was supported primarily by grants NSF/EAR 1319368 and NSF/CAREER 1151738. Han Hsu was supported by NSC 102-2112-M-008-001-MY3. Zhongqing Wu was supported by State Key Development Program of Basic Research of China (2014CB845905 and NSF of China (41274087). Computations were performed at the Minnesota Supercomputing Institute (MSI) and at the Blue Waters System at NCSA. The data for this paper are available at http://www.vlab.msi.umn.edu/reports/gauravpublications/index.shtml.

The Editor thanks two anonymous reviewers for their assistance in evaluating this paper.

References

Aizawa, Y., A. Yoneda, T. Katsura, E. Ito, T. Saito, and I. Suzuki (2004), Temperature derivatives of elastic moduli of $MgSiO_3$ perovskite, *Geophys. Res. Lett.*, *31*, L01602, doi:10.1029/2003GL018762.

Andrault, D., N. Bolfan-Casanova, and N. Guignot (2001), Equation of state of lower mantle (Al, Fe)-$MgSiO_3$ perovskite, *Earth Planet. Sci. Lett.*, *193*, 501–508.

Antonangeli, D., J. Siebert, C. M. Aracne, D. L. Farber, A. Bosak, M. Hoesch, M. Krisch, F. J. Ryerson, G. Fiquet, and J. Badro (2011), Spin crossover in ferropericlase at high pressure: A seismologically transparent transition?, *Science*, *331*, 64–67.

Badro, J., G. Fiquet, F. Guyot, J. P. Rueff, V. V. Struzhkin, G. Vank, and G. Monaco (2003), Iron partitioning in Earth's mantle: Toward a deep lower mantle discontinuity, *Science*, *300*, 789–791.

Badro, J., J. P. Rueff, G. Vanko, G. Monaco, G. Fiquet, and F. Guyot (2004), Electronic transitions in perovskite: Possible nonconvecting layers in the lower mantle, *305*(5682), 383–386.

Baroni, S., S. de Gironcoli, A. Dal Corso, and P. Giannozzi (2001), Phonons and related crystal properties from density-functional perturbation theory, *Rev. Mod. Phys.*, *73*(2), 515–562.

Bengtson, A., J. Li, and D. Morgan (2009), Mössbauer modeling to interpret the spin state of iron in (Mg, Fe)SiO_3, *Geophys. Res. Lett.*, *36*, L15301, doi:10.1029/2009GL038340.

Boehler, R. (2000), High-pressure experiments and the phase diagram of lower mantle and core materials, *Rev. Geophys.*, *38*(2), 221–245, doi:10.1029/1998RG000053.

Boffa Ballaran, T., A. Kurnosov, K. Glazyrin, D. J. Frost, M. Merlini, M. Hanfland, and R. Caracas (2012), Effect of chemistry on the compressibility of silicate perovskite in the lower mantle, *Earth Planet. Sci. Lett.*, *333-334*, 181–190, doi:10.1016/j.epsl.2012.03.029.

Caracas, R., H. Ishii, M. Hiraoka, Y. Ohishi, and N. Hirao (2014), Identifying the spin transition in Fe^{2+}-rich $MgSiO_3$ perovskite from X-ray diffraction and vibrational spectroscopy, *Am. Mineral.*, *99*(7), 1270–1276, doi:10.2138/am.2014.4783.

Carrier, P., R. M. Wentzcovitch, and J. Tsuchiya (2007), First principles prediction of crystal structures at high temperatures using the quasiharmonic approximation, *Phys. Rev. B: Condens. Matter*, *76*, 064116, doi:10.1103/PhysRevB.76.064116.

Ceperley, D. M., and B. J. Alder (1980), Ground state of the electron gas by a stochastic method, *Phys. Rev. Lett.*, *45*, 566–569.

Chantel, J., D. J. Frost, C. A. McCammon, Z. Jing, and Y. Wang (2012), Acoustic velocities of pure and iron-bearing magnesium silicate perovskite measured to 25 GPa and 1200 K, *Geophys. Res. Lett.*, *39*, L19307, doi:10.1029/2012GL053075.

Cococcioni, M., and S. de Gironcoli (2005), Linear response approach to the calculation of the effective interaction parameters in the LDA + U method, *Phys. Rev. B: Condens. Matter*, *71*, 035105.

Crowhurst, J. C., J. M. Brown, A. F. Goncharov, and S. D. Jacobsen (2008), Elasticity of (Mg, Fe)O through the spin transition of iron in the lower mantle, *Science*, *319*, 451–453, doi:10.1126/science.1149606.

da Silva, P., C. R. S. da Silva, and R. M. Wentzcovitch (2008), Metadata management for distributed first principles calculations in VLab—A collaborative cyberinfrastructure for materials computation, *Comput. Phys. Commun.*, *178*, 186–198, doi:10.1016/j.cpc.2007.09.001.

Dorfman, S. M., Y. Meng, V. B. Prakapenka, and T. S. Duffy (2013), Effects of Fe-enrichment on the equation of state and stability of (Mg, Fe)SiO_3 perovskite, *Earth Planet. Sci. Lett.*, *361*, 249–257.

Dziewonski, A. M., and D. L. Anderson (1981), Preliminary reference Earth model, *Phys. Earth Planet. Inter.*, *25*, 297–356.

Fiquet, G., A. Dewaele, D. Andrault, M. Kunz, and T. L. Bihan (2000), Thermoelastic properties and crystal structure of $MgSiO_3$ perovskite at lower mantle pressure and temperature conditions, *Geophys. Res. Lett.*, *27*(1), 21–24.

Floris, A., S. de Gironcoli, E. K. U. Gross, and M. Cococcioni (2011), Vibrational properties of MnO and NiO from DFT + U-based density functional perturbation theory, *Phys. Rev. B: Condens. Matter*, *84*, 161102(R).

Goncharov, A. F., V. V. Struzhkin, and S. D. Jacobsen (2006), Reduced radiative conductivity of low-spin (Mg, Fe)O in the lower mantle, *Science*, *312*, 1205–1208, doi:10.1126/science.1125622.

Himmetoglu, B., A. Floris, S. de Gironcoli, and M. Cococcioni (2014), Hubbard-corrected DFT energy functionals: The LDA + U description of correlated systems, *Int. J. Quantum Chem.*, *114*, 14–49, doi:10.1002/qua.24521.

Hohenberg, P., and W. Kohn (1964), Inhomogeneous electron gas, *Phys. Rev. B: Condens. Matter*, *136*, 864–871.

Hsu, H., and R. M. Wentzcovitch (2014), First-principles study of intermediate-spin ferrous iron in the Earth's lower mantle, *Phys. Rev. B: Condens. Matter*, *90*(19), 195205, doi:10.1103/PhysRevB.90.195205.

Hsu, H., K. Umemoto, M. Cococcioni, and R. M. Wentzcovitch (2009), First principles study of low-spin $LaCoO_3$ with structurally consistent Hubbard U, *Phys. Rev. B: Condens. Matter*, *79*, 125124, doi:10.1103/PhysRevB.79.125124.

Hsu, H., K. Umemoto, R. M. Wentzcovitch, and P. Blaha (2010), Spin states and hyperfine interactions of iron in (Mg, Fe)SiO_3 perovskite under pressure, *Earth Planet. Sci. Lett.*, *294*, 19–26, doi:10.1016/j.epsl.2010.02.031.

Hsu, H., P. Blaha, M. Cococcioni, and R. M. Wentzcovitch (2011), Spin-state crossover and hyperfine interactions of ferric iron in $MgSiO_3$ perovskite, *Phys. Rev. Lett.*, *106*, 118501, doi:10.1103/PhysRevLett.106.118501.

Jackson, J. M., J. Zhang, and J. D. Bass (2004), Sound velocities and elasticity of aluminous $MgSiO_3$ pervoskite: Implications for aluminum heterogeneity in Earth's lower mantle, *Geophys. Res. Lett.*, *31*, L10614, doi:10.1029/2004GL019918.

Jackson, J. M., W. Sturhahn, G. Shen, J. Zhao, M. Y. Hu, D. Errandonea, J. D. Bass, and Y. Fei (2005a), A synchrotron Mössbauer spectroscopy study of (Mg, Fe)SiO_3 perovskite up to 120 GPa, *Am. Mineral.*, *90*, 199–205.

Jackson, J. M., J. Zhang, J. Shu, S. V. Sinogeikin, and J. D. Bass (2005b), High-pressure sound velocities and elasticity of aluminous $MgSiO_3$ perovskite to 45 GPa: Implications for lateral heterogeneity in Earth's lower mantle, *Geophys. Res. Lett.*, *32*, L21305, doi:10.1029/2005GL023522.

Karki, B. B., R. M. Wentzcovitch, S. de Gironcoli, and S. Baroni (1999), First principles determination elastic anisotropy and wave velocities of MgO at lower mantle conditions, *Science*, *286*(5445), 1705–1707.

Karki, B. B., R. M. Wentzcovitch, S. de Gironcoli, and S. Baroni (2001), First principles thermoelasticity of $MgSiO_3$-perovskite: Consequences for the inferred properties of the lower mantle, *Geophys. Res. Lett.*, *28*, 2699–2702.

Kiefer, B., L. Stixrude, and R. M. Wentzcovitch (2002), Elasticity of (Mg, Fe)SiO_3-perovskite at lower mantle conditions, *Geophys. Res. Lett.*, *29*(11), 34-1–34-4, doi:10.1029/2002GL014683.

Kohn, W., and L. J. Sham (1964), Self-consistent equations including exchange and correlation effects, *Phys. Rev. A: At. Mol. Opt. Phys.*, *140*, 1133–1138.

Kulik, H., M. Cococcioni, D. A. Scherlis, and N. Marzari (2006), Density functional theory in transition metal chemistry: A self-consistent Hubbard U approach, *Phys. Rev. Lett.*, *97*, 103001.

Kupenko, I., C. McCammon, R. Sinmyo, C. Prescher, A. I. Chumakov, A. Kantor, R. Rüffer, and D. Dubrovinsky (2014), Electronic spin state of Fe, Al-containing $MgSiO_3$ perovskite at lower mantle conditions, *Lithos*, *189*, 167–172, doi:10.1016/j.lithos.2013.10.022.

Leiria Campo, V., Jr., and M. Cococcioni (2010), Extended DFT + U + V method with on-site and inter-site electronic interactions, *J. Phys. Condens. Matter*, *22*, 055602, doi:10.1088/0953-8984/22/5/055602.

Li, B., and J. Zhang (2005), Pressure and temperature dependence of elastic wave velocity of $MgSiO_3$ perovskite and the composition of the lower mantle, *Phys. Earth Planet. Inter.*, *151*, 143–154, doi:10.1016/j.pepi. 2005.02.004.
Li, J., V. V. Struzhkin, H. K. Mao, J. Shu, R. J. Hemley, Y. Fei, B. Mysen, P. Dera, V. Prakapenka, and G. Shen (2004), Electronic spin state of iron in lower mantle perovskite, *Proc. Natl. Acad. Sci.*, *101*, 14,027–14,030.
Li, J., W. Sturhahn, J. M. Jackson, V. V. Struzhkin, J. F. Lin, J. Zhao, H. K. Mao, and G. Shen (2006), Pressure effect on the electronic structure of iron in (Mg, Fe)(Si, Al)O_3 perovskite: A combined synchrotron Mossbauer and X-ray emission spectroscopy study up to 100 GPa, *Phys. Chem. Miner.*, *33*, 575–585.
Lin, J. F., E. E. Alp, Z. Mao, T. Inoue, C. McCammon, Y. Xiao, P. Chow, and J. Zhao (2012), Electronic spin and valence states of iron in the lower-mantle silicate perovskite by synchrotron Mössbauer spectroscopy, *Am. Mineral.*, *97*, 592–597.
Lundin, S., L. Catalli, J. Santillan, S.-H. Shim, V. B. Prakapenka, M. Kunz, and Y. Meng (2008), Effect of Fe on the equation of state of mantle silicate perovskite over 1 Mbar, *Phys. Earth Planet. Inter.*, *168*, 97–102.
Marquardt, M., S. Speziale, H. J. Reichmann, D. J. Frost, F. R. Schilling, and E. J. Garnero (2009), Elastic shear anisotropy of ferropericlase in Earth's lower mantle, *Science*, *324*, 224–226, doi:10.1126/science.1169365.
Marton, F. C., and R. E. Cohen (2002), Constraints on lower mantle composition from molecular dynamics simulations of $MgSiO_3$ perovskite, *Phys. Earth Planet. Inter.*, *134*, 239–252.
McCammon, C., I. Kantor, O. Narygina, J. Rouquette, U. Ponkratz, I. Sergueev, M. Mezouar, V. Prakapenka, and L. Dubrovinsky (2008), Stable intermediate-spin ferrous iron in lower-mantle perovskite, *Nat. Geosci.*, *1*, 684–687.
McCammon, C., et al. (2013), Iron spin state in silicate perovskite at conditions of the Earth's deep interior, *High Pressure Res.*, *43*(3), 663–672.
Murakami, M., S. V. Sinogeikin, H. Hellwig, J. D. Bass, and J. Li (2007), Sound velocity of $MgSiO_3$ perovskite to Mbar pressure, *Earth Planet. Sci. Lett.*, *256*, 47–54, doi:10.1016/j.epsl.2007.01.011.
Murakami, M., Y. Ohishi, N. Hirao, and K. Hirose (2012), A perovskitic lower mantle inferred from high-pressure, high-temperature sound velocity data, *Nature*, *485*, 90–94, doi:10.1038/nature11004.
Nunez-Valdez, M., Z. Wu, Y. G. Yu, J. Revenaugh, and R. M. Wentzcovitch (2012a), Thermoelastic properties of ringwoodite $(Fe_xMg_{1-x})_2SiO_4$: Its relationship to the 520 km seismic discontinuity, *Earth Planet. Sci. Lett.*, *351-352*, 115–122.
Nunez-Valdez, M., K. Umemoto, and R. M. Wentzcovitch (2012b), Elasticity of diamond at high pressures and temperatures, *Appl. Phys. Lett.*, *101*, 170912, doi:10.1063/1.4754548.
Nunez-Valdez, M., Z. Wu, Y. G. Yu, and R. M. Wentzcovitch (2013), Thermal elasticity of $(Fe_xMg_{1-x})_2SiO_4$ olivine and wadsleyite, *Geophys. Res. Lett.*, *40*, 290–294, doi:10.1002/grl.50131.
Oganov, A. R., J. P. Brodholt, and G. D. Price (2001), The elastic constants of $MgSiO_3$ perovskite at pressure and temperatures of the Earth's mantle, *Nature*, *411*, 934–9370, doi:10.1038/35082048.
Potapkin, V., et al. (2013), Effect of iron oxidation state on the electrical conductivity of the Earth's lower mantle, *Nat. Commun.*, *4*, 1427.
Sinnelnikov, Y. D., G. Chen, D. R. Neuville, M. T. Vaughan, and R. C. Liebermann (1998), Ultrasonic shear wave velocities of $MgSiO_3$ perovskite at 8 GPa and 800 K and lower mantle composition, *Science*, *281*, 667–679.
Sinogeikin, S. V., J. Zhang, and J. D. Bass (2004), Elasticity of single crystal and polycrystalline $MgSiO_3$ perovskite by Brillouin spectroscopy, *Geophys. Res. Lett.*, *31*, L06620, doi:10.1029/2004GL019559.
Tsuchiya, T., R. M. Wentzcovitch, C. R. S. da Silva, and S. de Gironcoli (2006), Spin transition in Magnesiowüstite in Earth's lower mantle, *Phys. Rev. Lett.*, *96*(19), 198501.
Umemoto, K., R. M. Wentzcovitch, Y. Yu, and R. Requist (2008), Spin transition in (Mg, Fe)SiO_3 perovskite under pressure, *Earth Planet. Sci. Lett.*, *276*, 198–206, doi:10.1016/j.epsl.2008.09.025.
Vanderbilt, D. (1990), Soft self-consistent pseudopotentials in a generalized eigenvalue formalism, *Phys. Rev. B: Condens. Matter*, *41*, 7892–7895.
Wentzcovitch, R. M. (1991), Invariant molecular dynamics approach to structural phase transitions, *Phys. Rev. B: Condens. Matter*, *44*, 2358–2361.
Wentzcovitch, R. M., J. L. Martins, and G. D. Price (1993), *Ab initio* molecular dynamics with variable cell shape: Application to $MgSiO_3$, *Phys. Rev. Lett.*, *70*, 3947.
Wentzcovitch, R. M., B. B. Karki, M. Cococcioni, and S. de Gironcoli (2004), Thermoelastic properties of $MgSiO_3$-perovskite: Insights on the nature of the Earth's lower mantle, *Phys. Rev. Lett.*, *92*, 018501.
Wentzcovitch, R. M., J. F. Justo, Z. Wu, C. R. S. da Silva, A. Yuen, and D. Kohlstedtd (2009), Anomalous compressibility of ferropericlase throughout the iron spin cross-over, *Proc. Natl. Acad. Sci.*, *106*(21), 8447–8452.
Wentzcovitch, R. M., Y. Yu, and Z. Wu (2010a), Thermodynamic properties and phase relations in mantle minerals investigated by first principles quasiharmonic theory, *Rev. Mineral. Geochem.*, *71*, 59–98.
Wentzcovitch, R. M., Z. Wu, and P. Carrier (2001b), First principles quasiharmonic thermoelasticity of mantle minerals, *Rev. Mineral. Geochem.*, *71*, 99–128.
Wu, Z., and R. M. Wentzcovitch (2011), Quasiharmonic thermal elasticity of crystals: An analytical approach, *Phys. Rev. B: Condens. Matter*, *83*, 184115.
Wu, Z., and R. M. Wentzcovitch (2014), Spin crossover in ferropericlase and velocity heterogeneities in the lower mantle, *Proc. Natl. Acad. Sci.*, *111*(29), 10,468–10,472.
Wu, Z., J. F. Justo, C. R. S. da Silva, S. de Gironcoli, and R. M. Wentzcovitch (2009), Anomalous thermodynamic properties in ferropericlase throughout its spin crossover, *Phys. Rev. B: Condens. Matter*, *80*, 014409.
Wu, Z., J. F. Justo, and R. M. Wentzcovitch (2013), Elastic anomalies in a spin-crossover system: Ferropericlase at lower mantle conditions, *Phys. Rev. Lett.*, *110*, 228501.
Yang, R., and Z. Wu (2014), Elastic properties of stishovite and the $CaCl_2$-type silica at the mantle temperature and pressure: An ab initio investigation, *Earth Planet. Sci. Lett.*, *404*, 14–21.
Yeganeh-Haeri, A. (1994), Synthesis and re-investigation of the elastic properties of single-crystal magnesium silicate perovskite, *Phys. Earth Planet. Inter.*, *87*, 111–121.
Zhang, L., et al. (2014), Disproportionation of (Mg, Fe)SiO_3 perovskite in Earth's deep lower mantle, *Science*, *344*(6186), 877–882.
Zhang, Z., L. Stixrude, and J. Brodholt (2013), Elastic properties of $MgSiO_3$-perovskite under lower mantle conditions and the composition of the deep Earth, *Earth Planet. Sci. Lett.*, *379*, 1–12.